J. Phys. B: At. Mol. Opt. Phys. **41** (2008) 125704 (9pp) doi:10.1088/0953-4075/41/12/125704

Femtosecond optical diagnostics and hydrodynamic simulation of Ag plasma created by laser irradiation of a solid target

M E Veysman, M B Agranat, N E Andreev, S I Ashitkov, V E Fortov, K V Khishchenko, O F Kostenko, P R Levashov, A V Ovchinnikov and D S Sitnikov

Joint Institute for High Temperatures, Russian Academy of Sciences, Izhorskaya 13 bldg 2, Moscow 125412, Russia

E-mail: bme@ihed.ras.ru

Received 12 January 2008, in final form 14 May 2008
Published 9 June 2008
Online at stacks.iop.org/JPhysB/41/125704

Abstract

A combined experimental–theoretical method of diagnostics of the plasma created on a surface of Ag target irradiated by intense femtosecond laser pulses is proposed. The method is based on semiempirical wide-range models of optical, transport and thermodynamic properties of Ag plasma. Numerical coefficients in these models are chosen so as to ensure the best accordance of simulations to measurements of a complex absorption coefficient of Ag plasma by means of femtosecond interference microscopy. A two-temperature hydrodynamic modelling of non-stationary laser-produced Ag plasma is carried out; calculated results are presented in comparison with experiments. Unexpectedly high values of the phase of the complex reflection coefficient at short (200 fs) time delay between pump and probe laser pulses are obtained experimentally; possible explanations of this phenomenon are discussed.

(Some figures in this article are in colour only in the electronic version)

1. Introduction

In all cases, when a laser pulse with power sufficient for ionization acts on a metal target, the matter on the target surface goes through complex modifications from its initial metallic state to the so-called disordered state [1], further to the states of degenerate and non-degenerate strongly coupled plasma and finally (if the laser power is high enough) to the state of weakly coupled plasma [2]. Though the lifetime of these states can be different for various parameters of irradiating laser pulses, in the general case for adequate description of irradiated-target characteristics and their temporal evolution the wide-range models of optical, transport and thermodynamic properties of matter are necessary. The role of modelling is especially important as the strong inhomogeneity of the produced plasma and its fast evolution does not permit the direct measurements of such plasma properties in experiments.

Many publications to date deal with models and simulations of dense laser-produced plasmas [3–11]. Rather sophisticated models of effective frequency of electron collisions [12–20], inverse-bremsstrahlung heating [15–20], permittivity of plasma [19–21], electron–ion relaxation rate [14, 22–25], thermal conductivity [7, 13, 24, 26], ionization equilibrium [27, 28], ionization rate [1, 4] and equation of state (EOS) [29] are presented in publications. However, it is difficult to use most of these models because of their complexity and (or) the restricted range of plasma parameters, in which the models can be applicable. Most models take into account some particular mechanisms of physical phenomena, often omitting other effects that occur in the processes of laser–matter interaction. The traditional solution of this problem is to use semiempirical models in order to describe the behaviour of generated plasma over a wide range of densities and temperatures [2, 30–33]. Such models provide

known analytical limits for the metallic state and for the weakly coupled plasma, while in the intermediate region of parameters they use interpolation functions with numerical constants determined from experimental data.

The semiempirical models for effective frequency of collisions of electrons were constructed and implemented recently for Au plasma [32]. More advanced semiempirical models of thermophysical properties over a wide range of parameters were worked out for Al [33]. The aim of the present work is to apply similar ideas for the study of Ag plasma. The main distinction of Ag from Al is that the ionization processes in the former case can occur at much lower temperatures (several electron-volts). There are three electrons (per atom) in the conductivity zone of Al under normal conditions, while just one electron is initially present in the conductivity zone of Ag. The necessity to account for the ionization process requires the introduction of additional numerical coefficients into semiempirical models. Besides at the considered wavelength of laser radiation (from 0.4 to 1.5 μm) interband transitions [14, 34] do not contribute to the absorption coefficient of Ag unlike Al plasma. Moreover, substantial distinction in the atomic weights $A = 27$ (Al) and 108 (Ag) should lead to a lower expansion rate of Ag than that of Al plasma at the equal average ion charges Z in accordance with the estimate of the velocity of expansion

$$V \sim \sqrt{ZT_e/m_i}, \tag{1}$$

where T_e is the temperature of electrons and m_i is the mass of ions.

The only experimental method, which could ensure the diagnostics of a laser produced plasma at the femtosecond time scale, is the optical method based on measurements of the reflection coefficient of some weak probe laser pulse from the plasma produced by an intense pump laser pulse. As in our previous paper [33], we use the method of femtosecond interference microscopy, which permits us to measure not only the module $|r|$, but also the phase Ψ of complex reflection coefficient r of the probe pulse from the matter heated by the pump pulse. Earlier, similar methods of measurement of Ψ were successfully used in some works [10, 35, 36].

The dependence of the module $|r|$ upon the time delay between femtosecond pump and probe laser pulses for Ag plasmas was studied in [37] for moderate pump laser intensity $I \sim 10^{13}$ W cm^{-2}. However, the measurements of dynamics of Ψ and its dependences on the pump laser pulse parameters can give additional important information, which is necessary for testing and determination of numerical coefficients in proposed wide-range semiempirical models of optical, transport and thermodynamic properties of matter under study.

2. Experiment

A source of radiation is a terawatt chromium-doped forsterite laser system that generates femtosecond pulses at the wavelength of 1.24 μm and repetition rate 10 Hz [38]. The full-width at half-maximum (FWHM) pulse duration measured using a non-collinear second harmonic autocorrelator was

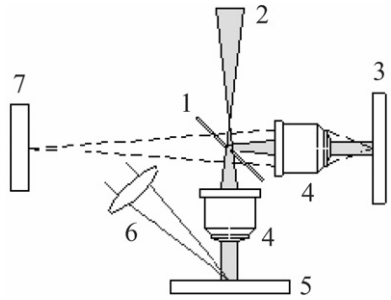

Figure 1. Optical measurement scheme: (1) the beam splitter plate, (2) the probe pulse, (3) the reference mirror, (4) the micro-objectives, (5) the target, (6) the pump pulse and (7) the CCD matrix.

100 fs. The shape of the temporal pulse profile was approximated as sech^2. Measurements of the high dynamic range temporal profile of the pulse were carried out using the correlator of the third harmonic. The pulse power contrast was not less than 10^4 at 1 ps before the pulse peak and more than 10^6 at 2 ps before the pulse peak [39].

In the present experiments the ultrafast image interferometry technique with Fourier processing of interference patterns [40] was used. The scheme of optical measurements is shown in figure 1.

The p-polarized pump pulses at the fundamental wavelength $\lambda_1 = 1.24$ μm were focused on a target using a 150 mm lens at the angle of incidence 45° in air. As was shown in [36, 41], atmospheric air does not appreciably disturb the results of such measurements at laser intensities up to 10^{14} W cm^{-2}. The energy of pump pulses was varied with the use of a half-wave plate in conjunction with an optical polarizer. For each laser shot the energy of the pump was measured by the calibrated photodiode. The spatial distribution of the pump pulse fluence over the target had the Gaussian shape with the beam diameter $d_0 = 70$ μm at the level of $\exp(-2)$.

The experiments were performed with Ag films of 5 μm thickness on silica substrates. The targets were mounted at the computer-controlled three-axis translation stage. After each pump shot the target was moved to a new area for irradiation focusing.

For the experimental study of optical properties of the excited area of a target the Michelson interferometer was used (see figure 1). The normally incident s-polarized probe pulse at the second harmonic wavelength $\lambda_2 = 0.62$ μm illuminated the heated area of the target with varying time delay after the pump pulse. The probe pulse intensity was about 5×10^{10} W cm^{-2}. The image of the target surface was transferred to the plane of a charge-coupled device (CCD) camera with the matrix 1024×1024 pixels and capacity of 12 bit by means of a micro-objective with the numerical aperture of $N_A = 0.2$. The second reference arm of the interferometer included a similar objective and a dielectric mirror. A narrow band filter cut the thermal radiation of the plasma. The probe beam (object) reflected from the sample interfered with the reference beam and formed the interference fringes in the CCD matrix plane.

In the experiments laser-induced changes of amplitude $r_{\mathrm{ind}}(x, y) = r_t(x, y)/r_i(x, y)$ and phase $\Psi_{\mathrm{ind}}(x, y) =$

$\Psi_t(x, y) - \Psi_i(x, y)$ of the reflected probe wave from the excited area of the target were measured. Here $r_i(x, y)$ and $\Psi_i(x, y)$ are the amplitude and the phase of the reflected probe wave from the target surface before the action of the pump pulse; $r_t(x, y)$ and $\Psi_t(x, y)$ are the amplitude and phase after the action of the pump pulse. The algorithm of 2D Fourier processing of interference patterns was described previously in [40, 42]. The accuracy of measurements of the amplitude and phase variations was better than 1% and $\pi/200$, correspondingly. The time resolution of the experimental setup was determined by the duration of the probe pulse (about 100 fs).

The crucial point in time-resolved experiments is the matching of pump and probe pulses in time. A zero delay was set when the peaks of the pump and probe laser pulses overlapped in time at the sample surface. To do this a Si sample with a fast temporal response of reflectivity was used. Under the action of the pump pulse with the intensity $I \sim 10^{12}$ W cm^{-2} electron–hole plasma formation occurred, which led to an increase of reflectivity of the Si sample [43].

The variations of r_{ind} and Ψ_{ind} as functions of the peak intensity I_1 of a heating laser pulse for various time delays between the pump and probe pulses are shown in figure 2. The presented values of r_{ind} and Ψ_{ind} were measured in the centre of the spot. Each experimental point is a result of averaging over five laser shots.

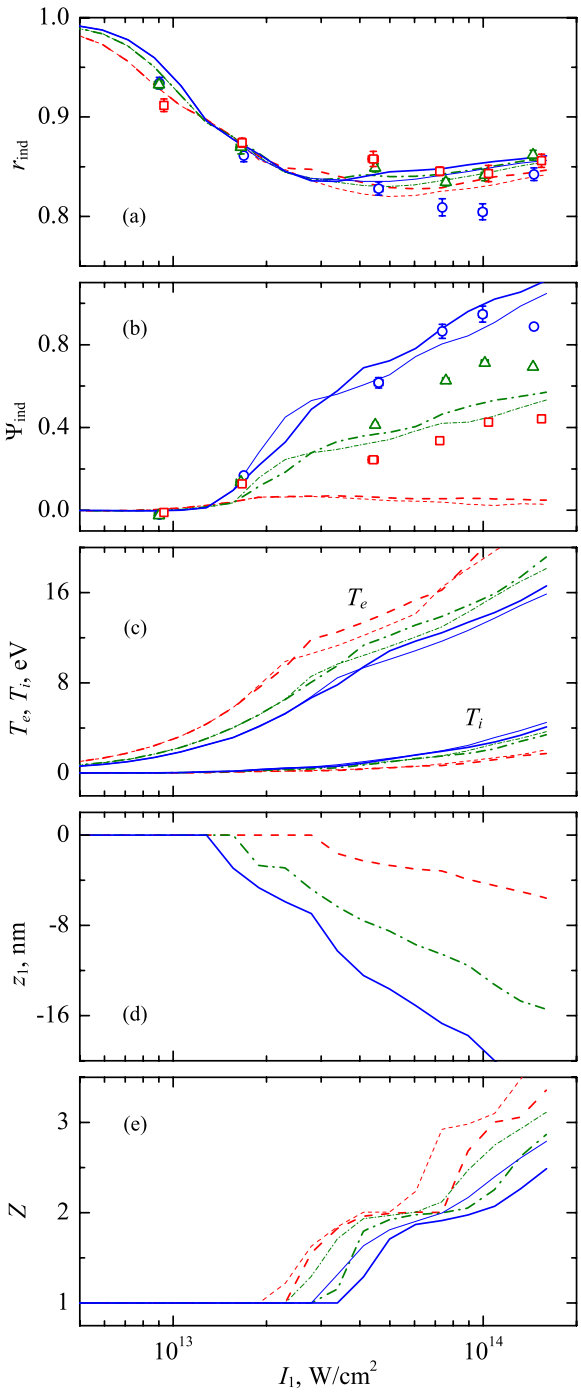

Figure 2. Experimental (markers) and calculated (lines) for Ag (a) r_{ind}, (b) Ψ_{ind}, (c) the temperatures of electrons T_e and heavy particles T_i at $z = 0$, (d) the position z_1 of the point at which the density ϱ_a of the plasma decreases to $\varrho_0 \exp(-1)$ (where $\varrho_0 = 10.5$ g cm^{-3} is the initial solid-state density of Ag) and (e) the average ion charge Z at $z = 0$ as functions of the peak intensity I_1 of the pump laser pulse for $\Delta t = 0.2$ (squares and dashed lines), 0.6 (triangles and dash-dot lines) and 1 ps (circles and solid lines). Thick and thin lines correspond to $k_U = 0.55$ and 0.35, respectively.

3. Theoretical model

The ionization, heating and expansion of plasma created on a solid target surface under the action of a pump laser pulse is described by the system of hydrodynamic equations [33, 44, 45] for the density of plasma ϱ_a, the average charge of ions Z, the velocity of quasi-neutral plasma V in the z direction perpendicular to the target and the energy (per particle) of electrons e^e and heavy particles (atoms, ions, nuclei) e^i,

$$\partial_t \varrho_a + \partial_z(\varrho_a V) = 0, \tag{2}$$

$$[\partial_t + V\partial_z]V = -\varrho_a{}^{-1}\partial_z(P_e + P_i) + F_p, \tag{3}$$

$$n_a[\partial_t + V\partial_z]e^i = -P_i\partial_z V + Q^{ei}, \tag{4}$$

$$Zn_a[\partial_t + V\partial_z]e^e = -\partial_z q_T - P_e\partial_z V - Q^{ei} - Q_Z + Q_{IB} - e^e\Theta, \tag{5}$$

$$[\partial_t + V\partial_z]Z = \Theta, \tag{6}$$

where P_e and P_i are the pressures of electrons and heavy particles in accordance with respective EOS; Θ and Q_Z are the full speed of thermal ionization and the density of power expended for ionization; $\varrho_a = m_i n_a$, $Z = n_e/n_a$, m_i is the heavy particle mass, n_a is the total concentration of heavy particles,

$$n_a = \sum_{q=0}^{z_n} n_q, \tag{7}$$

n_q is the concentration of ions with the charge q, z_n is the charge of nucleus and n_e is the concentration of electrons (quasi-neutrality is assumed),

$$n_e = \sum_{q=1}^{z_n} q n_q. \tag{8}$$

F_p is the ponderomotive force,

$$F_p = -K_1(\xi^\omega)\frac{Zm_e}{4m_i}\partial_z|\boldsymbol{V}_E|^2, \tag{9}$$

$\boldsymbol{V}_E \equiv e|\boldsymbol{E}|(m_e\omega_1)^{-1}$ is the quiver velocity of electrons under the laser irradiation with the slowly varying in time amplitude of the electric field $\boldsymbol{E}$ and the frequency ω_1, e and m_e are the electron charge and mass, $\xi^\omega = 3\sqrt{\pi}\nu_{\text{eff}}(4\omega)^{-1}$, ν_{eff} is the effective collision frequency of electrons, the function

$$K_1(x) = \frac{8}{3\sqrt{\pi}}\int_0^\infty \frac{t^{10}\exp(-t^2)}{t^6 + x^2}\,\mathrm{d}t \tag{10}$$

arises due to the integration of the velocity-dependent cross-section of electron–ion collisions over the Maxwell distribution function [44]; $Q^{ei} = \gamma^{ei}Zn_a(T_e - T_i)$ is the density of an electron–ion relaxation energy rate, T_e and T_i are the temperatures of electrons and heavy particles, respectively. The factor γ^{ei} is defined by the formula

$$\gamma^{ei} = 3(m_e/m_i)\nu_{\text{eff},\gamma}, \tag{11}$$

where the effective collision frequency of electrons $\nu_{\text{eff},\gamma}$ is determined so as to ensure the handbook value of $\gamma^{ei}(T_0)$ at the room temperature T_0 and to give the proper limit of γ^{ei} at high temperatures, where $\nu_{\text{eff},\gamma} = \nu_{\text{eff}}$, see below. The electronic thermal flux is set as

$$q_T = K'T_e\partial_z T_e, \tag{12}$$

where the factor K' is defined by the formula [46],

$$K' = -128\kappa_z Zn_a/(3\pi m_e\nu_{\text{eff},T}). \tag{13}$$

The effective collision frequency of electrons $\nu_{\text{eff},T}$, which contributes to a thermal conductivity, is defined so as to ensure the handbook value of $K'(T_0)$ and to give the proper limit of K' at high temperatures, where $\nu_{\text{eff},T} = \nu_{\text{eff}}$, see below. The multiplier $\kappa_z \simeq 0.7$ accounts for the influence of electron–electron collisions on the heat conductivity at high temperatures

$$Q_{IB} = (8\pi)^{-1}\omega_1\,\mathrm{Im}\{\varepsilon(\omega_1)\}|\boldsymbol{E}|^2 \tag{14}$$

is the power density of an inverse-bremsstrahlung absorption rate, ω_1 is the frequency of the pump laser pulse, $\varepsilon(\omega_1)$ is the permittivity of matter[1] determined by equations (17)–(20), see below.

The slowly varying in time amplitude of the electric field strength $\boldsymbol{E} = E_x\boldsymbol{e}_x + E_z\boldsymbol{e}_z$ ($\boldsymbol{e}_x$ and $\boldsymbol{e}_z$ are the unit vectors, the plane $x0z$ is determined by the wave vector of incident radiation and the normal to the target surface, i.e. the direction $0z$) for the p-polarized pump laser pulse was expressed through the amplitude of the magnetic field $\boldsymbol{B} = B\boldsymbol{e}_y$ as $E_x = -\mathrm{i}/(\varepsilon(\omega_1)k_1)\partial_z B$, $E_z = -B\sin(\theta)/\varepsilon(\omega_1)$, $k_1 = \omega_1/c$, c is the velocity of light. The wave equation (with proper boundary conditions) for the laser magnetic field envelope $\boldsymbol{B}$ [48],

$$\begin{aligned}&\partial_z^2 B + k_1^2[\varepsilon(\omega_1) - \sin^2(\theta)]B - \partial_z[\ln\varepsilon(\omega_1)]\partial_z B = 0,\\ &\partial_z B|_{z=z_0} = \mathrm{i}\varepsilon(\omega_1)k_1\cos(\theta)[2E_L - B]|_{z=z_0},\ B|_{z\to\infty} = 0,\end{aligned} \tag{15}$$

was solved numerically. Here $E_L = \sqrt{8\pi I_L/c}$, $I_L = I_L(t)$ is the intensity of the incident laser pulse, θ is the angle of incidence (the angle between the direction $0z$ and the wave vector of incident radiation, $\theta = 45^\circ$ for the present experiments), the point $z = z_0 \leqslant 0$ is at the plasma–vacuum boundary position, and the laser pulse propagates from the left (before the laser heats up the target $z_0 = 0$, the target is at $z \geqslant 0$, i.e. at the right half-space).

Note that equations (14) and (15) describe also a collisionless resonance absorption, but in the discussed range of the pump laser intensities, $I_1 \leqslant 2\times10^{14}$ W cm^{-2}, for a high contrast laser pulse of 100 fs duration the characteristic scale length of the plasma density does not exceed a few nanometers and the electron plasma temperature is about 10 eV, see figures 2(c) and (d), and so laser absorption takes place at over-critical densities in the normal skin heating regime [49].

The complex reflection coefficient of a weak probe s-polarized laser pulse with a frequency ω_2 at normal incidence was determined in the linear approximation. For this goal the wave equation with boundary conditions for the single component of electric field of the probe laser pulse $\boldsymbol{E} = E(z)\boldsymbol{e}_y$ [48],

$$\begin{aligned}&\partial_z^2 E + k_2^2\varepsilon(\omega_2)E = 0, \qquad k_2 = \omega_2/c,\\ &\partial_z E|_{z=z_0} = \mathrm{i}k_2[2E_L - E]|_{z=z_0}, \qquad E_{z\to\infty} = 0,\end{aligned} \tag{16}$$

was solved numerically on the spatially non-uniform profiles of the permittivity $\varepsilon(\omega_2)$ for different time delays. Here $E_L = E_L(t)$ is the amplitude of the incident probe laser pulse. For each time delay the permittivity is determined by equations (17)–(20) (see below) with the help of a numerical solution of hydrodynamic equations (2)–(6) that describe the dynamics of a target irradiated by the pump laser pulse determined self-consistently by equation (15).

It should be noted that in equations (15) and (16) for subpicosecond laser pulses the transverse (to the normal of the target, $0z$) gradients of the fields and plasma permittivity, which are determined by the characteristic scale lengths of the order of 10 μm, can always be omitted in comparison with the longitudinal gradients, which are determined by the skin-layer depth of a typical size of the order of 10 nm.

The permittivity of matter $\varepsilon(\omega)$ for the frequency of the pump laser pulse ω_1 as well as for the probe pulse on the second harmonic ω_2 of the fundamental frequency was determined in such a way that it describes exactly the well-known asymptotic behaviour. For metallic plasma at relatively small temperatures $T_e \ll T_1 \lesssim T_{\text{F}}$ the permittivity can be determined by the Drude-like formula [50, 51],

$$\varepsilon_{\text{met}} = \varepsilon'_{\text{pb}} + \mathrm{i}\varepsilon''_{\text{pb}} + 1 - (n_e/n_c)(m_e/m_{\text{opt}})(1 + \mathrm{i}\nu_{\text{eff}}/\omega)^{-1}, \tag{17}$$

where $n_c = m_e\omega^2/[4\pi e^2]$, m_{opt} is the optical mass of the electron, $T_{\text{F}} = (3\pi^2 Zn_a)^{2/3}\hbar^2/(2m_e)$ is the Fermi temperature. At relatively high temperatures $T_e \gg T_2 \gtrsim T_{\text{F}}$ the permittivity can be determined by the expression

$$\varepsilon_{\text{pl}} = 1 - (n_e/n_c)[K_1(\xi^\omega) - \mathrm{i}(\nu_{\text{eff}}/\omega)K_2(\xi^\omega)] \tag{18}$$

for weakly coupled non-degenerate plasma [44, 45, 52], where the function

$$K_2(x) = 2\int_0^\infty \frac{t^7\exp(-t^2)}{t^6 + x^2}\,\mathrm{d}t \tag{19}$$

[1] The expression (14) is written in the approximation of weak spatial dispersion of permittivity [47], which is valid at temperatures $T < 1$ keV.

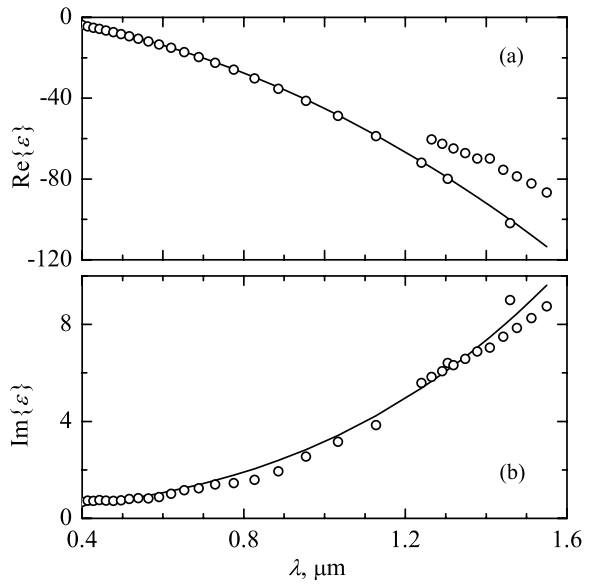

Figure 3. Calculated (lines) and handbook [34] (circles) values of (a) Re{ε} and (b) Im{ε} as functions of the wavelength of incident radiation λ for Ag at the room temperature.

contains an integration of the velocity-dependent collision frequency over the Maxwell distribution function [44]. Finally, in the present simulations over the whole temperature range, we defined the permittivity by the approximative formula

$$\varepsilon = \varepsilon_{\rm met} + \frac{1}{2}(\varepsilon_{\rm pl} - \varepsilon_{\rm met}) \tanh \frac{2T_e - (T_1 + T_2)}{2(T_2 - T_1)}, \qquad (20)$$

which gives smooth interpolation in the region $T_1 \lesssim T_e \lesssim T_2$ near the Fermi temperature $T_{\rm F}$ between the Drude-like permittivity (17) and the plasma permittivity (18). The coefficients $k_{T1} \lesssim k_{T2} \sim 1$, which relate the left and right boundaries of the interpolation region with the Fermy temperature, $T_1 = k_{T1}T_{\rm F}$, $T_2 = k_{T2}T_{\rm F}$, are the free parameters of the model.

In (17) the terms $\varepsilon'_{\rm pb}$ and $\varepsilon''_{\rm pb}$ are formed by the contribution of interband (parallel band) transitions to conductivity, while the other terms are stipulated by the Drude or intraband transitions [14, 51]. For the considered wavelengths and Ag target, $\varepsilon''_{\rm pb} = 0$ [34], while the parameter $\varepsilon'_{\rm pb}$ is nonzero due to the Kramers–Kronig relation,

$$\varepsilon'_{\rm pb}(\omega) = \frac{2}{\pi} \int_{\omega_{\rm cut}}^{\infty} \frac{\omega' \varepsilon''_{\rm pb}(\omega')}{\omega'^2 - \omega^2} \, {\rm d}\omega', \qquad (21)$$

where $\omega_{\rm cut}$ is the lower limit of a laser frequency, for which parallel band transitions make contribution to conductivity. In the case under consideration, $\omega < \omega_{\rm cut}$, one can disregard the dependence of $\varepsilon'_{\rm pb}$ upon ω, so that $\varepsilon'_{\rm pb} = {\rm const}$ [51].

From (17) with $\varepsilon'_{\rm pb} = {\rm const}$, $\varepsilon''_{\rm pb} = 0$ and the room-temperature optical constants of Ag taken from the handbook [34] (figure 3), one can infer $\varepsilon'_{\rm pb} = 2.85$, $m_{\rm opt}/m_e = 1.06$ and also the below approximation of $C_{e\cdot ph}$ (25). Note that the obtained value of the optical mass of electron is in good agreement with the available estimations $m_{\rm opt}/m_e \simeq 1$ for Ag [53].

When the temperature of the lattice T_i exceeds the melting boundary $T_{\rm melt}$, the zone structure of metals is destroyed and the contribution of interband transitions to conductivity also disappears [34]. This fact is taken into account by putting $m_{\rm opt} = m_e$ and $\varepsilon'_{\rm pb} = \varepsilon''_{\rm pb} = 0$ for $T_i > T_{\rm melt}$.

The effective collision frequency $\nu_{\rm eff}$ in the whole temperature range was defined by the approximative formula, which gives smooth interpolation between the metal limit $\nu_{\rm eff} \simeq \nu_{\rm met}$ at relatively low temperatures $T_e \lesssim T_{\rm F}$ and the limit $\nu_{\rm eff} \simeq \nu_{\rm pl}$ at high temperatures $T_e \gg T_{\rm F}$ and which restricts $\nu_{\rm eff}$ by some maximal value,

$$\nu_{\rm eff} = \nu_{\rm max}[1 + (\nu_{\rm max}/\nu_{\rm met})^6 + (\nu_{\rm max}/\nu_{\rm pl})^6]^{-1/6}, \qquad (22)$$

where $\nu_{\rm max}$ is the largest possible frequency of collisions, which is determined by the fact that the mean free path of electrons between collisions $\lambda_e \sim v_e/\nu_{\rm eff}$ (where v_e is the average speed of electrons) cannot be less than the average distance between ions $r_0 \sim n_a^{-1/3}$ [2, 54],

$$\nu_{\rm max} = k_1 \omega_{pe}, \qquad (23)$$

$\omega_{pe} = \sqrt{4\pi Z n_a e^2/m_e}$ is the electronic plasma frequency, the numerical factor $k_1 \lesssim 1$ is found from a comparison of the modelling results with the experimental data [33]; $\nu_{\rm met}$ is the effective collision frequency in metal plasma at $T_e \lesssim T_{\rm F}$,

$$\nu_{\rm met} = C_{e\cdot ph} T_i/\hbar + k_2 T_e^2/(\hbar T_{\rm F}). \qquad (24)$$

Two terms in (24) account for the contribution of electron–phonon [14, 50] and electron–electron [55] collisions, respectively. The constant k_2 is determined by a comparison of the results of simulations and measurements [32, 33]. The value $C_{e\cdot ph} = C_{e\cdot ph}(\omega)$ was determined from the data for room-temperature optical constants n and k, $n + {\rm i}k = \sqrt{\varepsilon}$, of Ag [34] and the expression for the permittivity of metallic plasma $\varepsilon_{\rm met}$ (17). In accordance with [51], the function $C_{e\cdot ph}(\omega)$ can be represented as $C_{e\cdot ph} = {\rm const}_1 + {\rm const}_2\omega^2$. From the comparison of the handbook data [34] and the calculated values of $\varepsilon(T_0)$ from (17), illustrated by figure 3, the value of $C_{e\cdot ph}$ for Ag in the range of laser-radiation wavelengths $0.4 \leqslant \lambda \leqslant 1.6$ μm can be approximated as

$$C_{e\cdot ph} = 2.2 + 0.28(\omega/10^{15})^2, \qquad (25)$$

where ω is measured in ${\rm s}^{-1}$.

The value

$$\nu_{\rm pl} = (4/3)\sqrt{2\pi} Z^2 n_a e^4 \Lambda/\sqrt{m_e T_e^3} \qquad (26)$$

is the frequency of collisions for weakly coupled plasma [52], Λ is the Coulomb logarithm. Despite simplicity of such an approach for the definition of $\nu_{\rm eff}$, it provides reasonable accuracy in comparison with much more complex models [18].

The value of $\nu_{{\rm eff},\gamma}$ in (11) is given by the same formulae (22)–(24), (26) as for $\nu_{\rm eff}$ but with the value of $C_{e\cdot ph} = {\rm const}$ determined from the equality $\gamma^{ei}(T_0) = 3.84 \times 10^{10}$ ${\rm s}^{-1}$ for Ag. Similarly, the value of $\nu_{{\rm eff},T}$ in (13) is given by formulae (22)–(24), (26) with the value of $C_{e\cdot ph} = {\rm const}$ determined from the equality $K'(T_0) = 7.28 \times 10^{36}$ (erg cm s)$^{-1}$ for Ag and with the substitution $k_{2,T}$ for k_2 in (24), where $k_{2,T}$ is one more free parameter of the model, which can be determined from experimental data (see also [32, 33]).

The full speed of thermal ionization Θ and the density of power expended for ionization Q_Z are determined within the

framework of an average ion model as

$$\Theta = Zn_a^2 \varkappa_z(\varrho_a, T_e, Z)[1 - Z/Z_{\rm eq}(\varrho_a, T_e)], \quad (27)$$

$$Q_Z = \Theta U(Z) - n_a \partial_z (V\partial/\partial n_a [\Sigma_U(Z) - \Sigma_U(Z_{\rm min})]), \quad (28)$$

where $Z_{\rm eq}$ is the equilibrium average ion charge, $Z_{\rm min} = Z_{\rm eq}(\varrho_a, 0)$ is the initial average charge of ions at a given-density point, $Z_{\rm min} = 1$ for Ag under normal conditions. The first term on the right-hand side of (27) determines the rate of collisional ionization, while the term proportional to $Z/Z_{\rm eq}$ accounts for the 3-body recombination via the detailed balance principle. The total energy of Z-fold ionization of a neutral atom is defined as

$$\Sigma_U(Z) = \int_0^Z U(Z')\,{\rm d}Z', \quad (29)$$

where $U(Z)$ is the ionization potential of the average ion with the charge Z,

$$U(Z) = U_{[Z]+1}\Delta Z + U_{[Z]}(1 - \Delta Z), \quad (30)$$

where $[Z]$ denotes the integer part of Z, $\Delta Z = Z - [Z]$, $U_0 = 0$; U_l with $l = 1, \ldots, z_n$ are the potentials of l-fold ionization, which are determined as

$$U_l(\varrho_a) = \Phi_l + \Delta\Phi_l(\varrho_a), \quad (31)$$

where Φ_l is the tabulated value of the ionization potential for an isolated $(l-1)$-fold ion, $\Delta\Phi_l$ accounts for the lowering of ionization potentials in a dense medium. As far as we know, there is no reliable enough formula for $\Delta\Phi_l$ in the dense plasma until now [2]. Keeping in mind that according to [27, 28] the lowering of an ionization potential should be inversely proportional to the inter-atomic distance, and that the dense medium should influence more on the outer-shell electrons than on the inner-shell ones, we can write the following expression for $\Delta\Phi_l$,

$$\Delta\Phi_l(\varrho_a) = -\Phi_l[\varrho_a/\varrho_0]^{1/3}(1 - \min\{k_U l^{\beta_U}, 1\}), \quad (32)$$

where ϱ_0 is the normal (solid) density of matter, k_U and β_U are the free parameters, which can be determined from the comparison with the experiment.

Taking into account formula (30) for U, one can obtain the following expression for Σ_U through (29),

$$\Sigma_U = ZU_1 + (Z-1)^2(U_2 - U_1)/2 \quad (33)$$

at $1 \leqslant Z \leqslant 2$,

$$\Sigma_U = U_1/2 + \sum_{l=1}^{q-1} U_l + (Z - q + 1/2)U_q + (Z-q)^2(U_{q+1} - U_q)/2 \quad (34)$$

at $q \leqslant Z \leqslant q+1$, where $q = 2, \ldots, z_n - 1$.

The ionization rate $\varkappa_z$ in (27) is determined by the model derived in [1] as

$$\varkappa_z(\varrho_a, T_e, Z) = A_\varkappa \xi(Z)\sqrt{U_{\rm H}/T_e}[U_{\rm H}/U(Z)]\mathfrak{I}(\varrho_a, T_e, Z), \quad (35)$$

where $A_\varkappa = 6 \times 10^{-8}$ cm^3 s^{-1}, ξ is the current (non-integer) number of electrons on the outer non-empty shell of an ion of average charge Z and $U_{\rm H}$ is the ionization potential of an isolated atom of hydrogen,

$$\mathfrak{I} = \frac{3\sqrt{\pi}}{4}\frac{\epsilon_z}{\epsilon_{\rm F}^{3/2}}\int_1^\infty \times \frac{\ln(t)(1-1/t)^{Y(\epsilon_{\rm F})}}{[1+\exp(\epsilon_z[1-t]/2+\epsilon_\mu)]^2[1+\exp(\epsilon_z t - \epsilon_\mu)]}\,{\rm d}t, \quad (36)$$

where $\epsilon_z = U(Z)/T_e, \epsilon_{\rm F} = T_{\rm F}/T_e, \epsilon_\mu = \mu/T_e, \mu = \mu(\varrho_a, T_e, Z)$ is the chemical potential of electrons. The value of ϵ_μ is determined by the equality

$$\epsilon_\mu = X_{1/2}\left(2\epsilon_{\rm F}^{3/2}/3\right), \quad (37)$$

where $X_{1/2}$ is the function reverse to the Fermi integral $F_{1/2}$,

$$F_{1/2}(x) = \int_0^\infty [1+\exp(t-x)]^{-1} t^{1/2}\,{\rm d}t, \quad (38)$$

so that $X_{1/2}(F_{1/2}(x)) \equiv x$. The function $X_{1/2}$ is calculated by a simple approximative formula derived in [56].

The empirical correction factor $(1-1/t)^Y$ in (36) accounts for the decrease of ionization cross-section in the dense medium due to the screening and continuum wavefunction modification effects [1]. This factor should decrease with the increase of temperature as well as decrease of density of plasma. This circumstance was accounted by the approximation

$$Y(\epsilon_{\rm F}) = Y_0\epsilon_{\rm F}/(1+\epsilon_{\rm F}), \quad (39)$$

where Y_0 is the room temperature value of Y, as it was introduced in [1]. In the limit $\epsilon_{\rm F} \to 0$ the value of integral (36) tends to $\mathfrak{I} \to {\rm Ei}(\epsilon_z)$,

$${\rm Ei}(x) = \int_{-\infty}^x t^{-1}\exp(t)\,{\rm d}t, \quad (40)$$

and the formula (35) transforms into the well-known Lotz expression [57].

The average equilibrium ion charge $Z_{\rm eq}$ was determined by the chemical model of degenerate plasma [27, 28] and is given by the solution of the following equation,

$$Z_{\rm eq}\left[1 + \sum_{q=1}^{z_n}\exp(-\Psi_q/T_i)\right] - \sum_{q=1}^{z_n} q\exp(-\Psi_q/T_i) = 0, \quad (41)$$

where

$$\Psi_q = q\mu(\varrho_a, T_i, Z_{\rm eq}) + \sum_{l=1}^{q} U_l(\varrho_a), \quad (42)$$

the chemical potential μ is calculated from (37), and the ionization potential U_l is determined in accordance with (31) and (32). The ion charge $Z_{\rm eq}$ was restricted from below by the value $Z_{\rm min} = 1$.

The EOS in the form of functions $e^e(\varrho_a, T_e, Z)$, $P_e(\varrho_e, T_e, Z)$, $e^i(\varrho_a, T_i)$ and $P_i(\varrho_a, T_i)$ described elsewhere [33] was adapted for Ag and used in the present simulations. It should be noted that for more precise description of the process of plasma expansion one should use the multi-phase EOS [58–60], which is much more complicated than the one-condensed-phase EOS [33]. To overcome this difficulty

and take into account the effect of changes of expansivity properties of matter under phase transitions, the artificial delay of the beginning of the target–surface movement was introduced while solving the system of equations (2)–(6) with the EOS [33]. Namely, the velocity of expansion V was zero until the temperature T_i on the target surface became higher than the evaporation temperature $T_{\rm vap} = 0.21$ eV of Ag.

4. Comparison of experimental and theoretical results and discussion

The simulation results as well as the obtained data for the relative module $r_{\rm ind}$ and phase $\Psi_{\rm ind}$ of the reflection coefficient of the probe laser pulse are shown in figure 2 for different time delays Δt between the pump and probe laser pulses.

The large number of free parameters ($k_1, k_2, k_{2,T}, k_U$, β_U, Y_0, k_{T1} and k_{T2}) of the model can give someone an impression that it is always possible to fit any experimental data by the appropriate choice of these parameters. However, for physically reasonable values of the parameters of the order of unity the influence of some of them on the reflection coefficient $r_{\rm ind}$ and the phase $\Psi_{\rm ind}$ of the probe laser pulse is insignificant, while the influence of others is restricted. The factors which have the strongest influence on $r_{\rm ind}$ and $\Psi_{\rm ind}$ are the expansion of the plasma, the absorption of the pump and probe laser radiation and the ionization of matter[2]. Note that the rate of expansion of the plasma is governed by the speed of sound, which is determined by the presently used EOS model.

The rate of laser energy absorption is determined by the coefficients k_1, k_2, k_{T1} and k_{T2} in formulae (23), (24) and (20). The comparison of experimental results with simulations performed on the basis of the theoretical model described in section 3 determines the values $k_1 \simeq 0.8, k_2 \simeq 0.75, k_{T1} \simeq 0.4$ and $k_{T2} \simeq 0.7$ within about 15% of accuracy. For values of k_1 bigger than stated above, the calculated values of $r_{\rm ind}$ at high pump laser fluxes are lower, while for smaller values of k_1 the resulting values of $r_{\rm ind}$ are higher than the experimental ones. A smaller value of k_2 leads to much lower than necessary values of $\Psi_{\rm ind}$, whereas a bigger value of k_2 tends to much higher values of $r_{\rm ind}$. The increase of the coefficients k_{T1} and k_{T2} leads to the decrease of $r_{\rm ind}$ at moderate laser fluxes of several units of 10^{13} W cm^{-2}. The value of $k_{2,T}$ has less influence on $r_{\rm ind}$ and $\Psi_{\rm ind}$ than the values of k_1, k_2, k_{T1} and k_{T2}. From a comparison with experiments, $k_{2,T} \simeq 1$ with the accuracy of about 30%.

The coefficient Y_0 influences strongly the rate of thermal ionization $\varkappa_Z$ in the dense plasmas, as one can see in figure 4. Nevertheless, the influence of Y_0 on $r_{\rm ind}$ and $\Psi_{\rm ind}$ is not significant. This is connected with the fact that in a dense plasma, which absorbs the largest part of laser radiation, the rate of thermal ionization is high enough for the ion charge Z to be equal to the equilibrium charge $Z_{\rm eq}$ for $\Delta t > 10$ fs. Only in the plasma corona the difference of Z and $Z_{\rm eq}$ is considerable, compare thick and thin lines in figure 5(c). The value of Y_0

[2] In our previous paper [33] the aluminium plasma was considered, for which the ionization played no role for moderate ($I_1 \lesssim 10^{14}$ W cm^{-2}) pump laser pulses because three electrons are initially already present in the conduction band of solid-state Al.

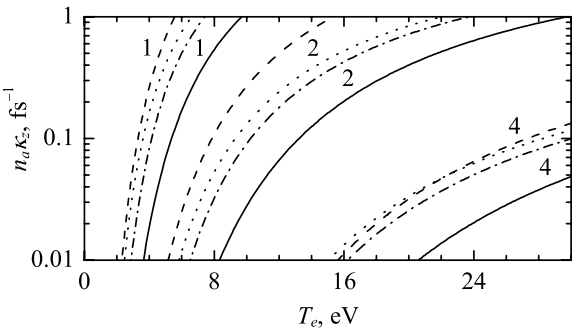

Figure 4. The ionization rate $n_a\varkappa_Z$ in Ag plasma at $\varrho_a = \varrho_0$ as a function of the electronic temperature T_e. Curves numbered as 1, 2 and 4 correspond to the ionization of 1-, 2- and 4-fold ions, respectively. The solid lines are calculated from (35) with $Y_0 = 2.5$ and $k_U = 0.55$, the dashed lines—$Y_0 = 2.5$ and $k_U = 0.35$, the dash-dot lines—$Y_0 = 0$ and $k_U = 0.55$; the dotted lines are obtained from the Lotz ionization formula [57] with $k_U = 0.55$.

was chosen to be equal to $Y_0 = 2.5$ in accordance with the affirmation that larger values of Y_0 correspond to materials with higher atomic weights [14]. On the other hand, the influence of k_U on $r_{\rm ind}$ and $\Psi_{\rm ind}$ is substantial, as long as this parameter directly determines the value of $Z_{\rm eq}$ via (31), (32) and (41). The results of calculations with two values $k_U = 0.55$ and 0.35 are shown in figure 2. The parameter β_U was equal to $\beta_U = 0.5$ in all cases; $r_{\rm ind}$ and $\Psi_{\rm ind}$ are not sensitive to its variation. The value $k_U = 0.55$ gives the calculated phases $\Psi_{\rm ind}$ closer to the experimental data at $\Delta t = 0.6$ ps, but leads to a too high value of $\Psi_{\rm ind}$ for $\Delta t = 1$ ps at large fluxes $I_1 > 10^{14}$ W cm^{-2}. In contrast, the value $k_U = 0.35$ ensures better agreement with experimental values of $\Psi_{\rm ind}$ for $\Delta t = 1$ ps, but worse agreement for $\Delta t = 0.6$ ps.

Note that the sharp increase of the phase $\Psi_{\rm ind}$ for $I_1 > 1.3 \times 10^{13}$ W cm^{-2} is directly related to the beginning of the plasma expansion. The expansion (without ionization, in the case of simulation at a constant average ion charge $Z = 1$) increases the phase $\Psi_{\rm ind}$, while the ionization (without expansion, in the case of simulation at constant density $\varrho_a = \varrho_0$) decreases it. In accordance with equation (1), the rate of expansion of Ag plasma should be smaller than that for Al plasma under similar experimental conditions. This is confirmed by the dynamics of Ψ variation with the delay Δt for $\Delta t > 0.2$ ps. In the case of Ag plasma, the maximal values of $\Psi_{\rm ind} \simeq 0.7$ for $\Delta t = 0.6$ ps and $\Psi_{\rm ind} \simeq 1$ for $\Delta t = 1$ ps (present work), while for Al plasma the maximal values of $\Psi_{\rm ind} \simeq 0.9$ for $\Delta t = 0.6$ ps and $\Psi_{\rm ind} \simeq 1.5$ for $\Delta t = 1$ ps [33], compare figure 2(b) in this paper and figure 3(b) in [33]. More complicated dependence of $\Psi_{\rm ind}$ upon both I_1 and Δt for Ag plasma in comparison with Al plasma is connected with ionization processes.

It should be stressed that for all physically reasonable variants of choice of the free parameters of the model for Ag, the experimental value of the phase $\Psi_{\rm ind}$ at the short time delay $\Delta t = 0.2$ ps is several times larger than the calculated one. From the above analysis, this could serve as an indication that in the present experiment the expansion of the plasma at $\Delta t = 0.2$ ps was considerably larger than follows from the theory.

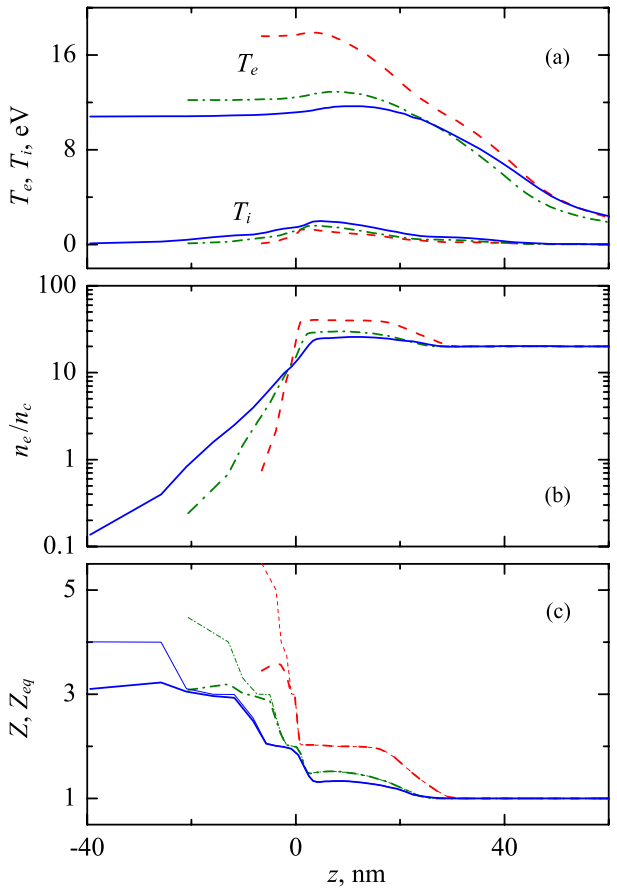

Figure 5. The calculated (a) temperatures of electrons T_e and heavy particles T_i, (b) the electronic concentration n_e normalized to the critical concentration n_c, (c) the current average ion charge Z (thick lines) and its equilibrium value Z_{eq} (thin lines) as functions of coordinate z normal to the irradiated surface of Ag target for the peak intensity of the pump laser pulse $I_1 = 7.5 \times 10^{13}$ W cm^{-2} at $\Delta t = 0.2$ (dashed lines), 0.6 (dash-dot lines) and 1 ps (solid lines), where $k_U = 0.55$.

From the recent papers [61, 62] it follows that the process of thermal excitation of d-electrons can affect considerably the kinetic coefficients of plasmas of noble metals. The account of the influence of thermal excitation of d-electrons on the optical properties of plasma created on the surface of an irradiated target will be the subject of our further theoretical study. Nevertheless, our preliminary calculations have shown that the account of d-electrons cannot explain too high values of Ψ_{ind} at short time delay $\Delta t = 0.2$ ps.

In principle, phase transitions in the target material can modify the optical properties of laser-produced plasmas [63] and thus can lead to a jump in Ψ_{ind}. But such a jump should be of similar value for all fluxes above some threshold value, whereas in the experiment Ψ_{ind} strongly increases with I_1, see figure 2(b).

From the above analysis we can conclude that if one excludes the possibility of some systematic experimental error, the only explanation for the unexpectedly high Ψ_{ind} at $\Delta t = 0.2$ ps could be larger expansion of the reflecting layer of the created plasma than it follows from our hydrodynamic analysis.

5. Conclusion

In this paper, the semiempirical models of optical, transport and thermodynamic properties of Ag plasma created during the action of a short laser pulse on an Ag target are proposed. These models include numerical coefficients chosen by a comparison of simulation results with data on the complex reflection coefficient of the irradiated Ag target from the measurements by means of the method of femtosecond interference microscopy. The advantage of this method is that it can give information not only on the module but also on the phase of the complex reflection coefficient depending on the time delay between the pump and probe pulse.

Unlike Al plasma, in Ag plasma ionization takes place even at moderate intensities (several units of 10^{13} W cm^{-2}) of laser pulses. It was shown that ionization as well as expansion of the plasma plays an important role in the dynamics of the reflection coefficient for Ag plasma. Therefore the proposed models were supplemented also by semiempirical expressions for the average charge of ions and ionization rate of Ag plasma.

The developed semiempirical models ensure the adequate description of the module and the phase of the complex reflection coefficient at all intensities of the pump laser flux and all time delays studied in the experiment except for the short ($\Delta t \sim 200$ fs) time delays, where unexpectedly high values of the phases Ψ_{ind} were measured. The origin of such high values of Ψ_{ind} at short time delays should be the subject of a further study.

Acknowledgments

The work was partially supported by the Russian Foundation for Basic Research (grants no. 07-02-92160 and 08-08-01055), the Council on Grants from the President of the Russian Federation (grant no. NSh-6494.2008.2) and the Presidium of the Russian Academy of Sciences (program no. P-9).

References

[1] Fisher D, Henis Z, Eliezer S and Meyer-ter-Vehn J 2006 *Laser Part. Beams* **24** 81–94
[2] Fortov V, Iakubov I and Khrapak A 2006 *Physics of Strongly Coupled Plasma* (Oxford: Oxford University Press)
[3] Anisimov S I, Prokhorov A M and Fortov V E 1984 *Sov. Phys.—Uspekhi* **27** 181–205
[4] Vinogradov A V and Shlyaptsev V N 1983 *Sov. J. Quantum Electron.* **13** 298–302
[5] Luther-Davies B, Gamaly E G, Wang Y, Rode A and Tikhonchuk V T 1991 *Laser Phys.* **1** 325–65
[6] Rozmus W, Tikhonchuk V T and Cauble R 1996 *Phys. Plasmas* **3** 360–7
[7] Anisimov S I and Rethfeld B 1997 *Proc. SPIE* **3093** 192–203
[8] Zhidkov A and Sasaki A 1999 *Phys. Rev.* E **59** 7085–95
[9] Eidmann K, Meyer-ter-Vehn J, Schlegel T and Hüller S 2000 *Phys. Rev.* E **62** 1202–14
[10] Widmann K *et al* 2001 *Phys. Plasmas* **8** 3869–72
[11] Chimier B, Tikhonchuk V T and Hallo L 2007 *Phys. Rev.* B **75** 195124
[12] Gurzhi R N 1959 *Sov. Phys.—JETP* **8** 673
[13] Yakovlev D G and Urpin V A 1980 *Sov. Astron.* **24** 303–10
[14] Fisher D, Fraenkel M, Henis Z, Moshe E and Eliezer S 2001 *Phys. Rev.* E **65** 016409

[15] Wierling A, Millat T, Röpke G, Redmer R and Reinholz H 2001 *Phys. Plasmas* **8** 3810–9
[16] Kurilenkov Y K, Berkovsky M A, Hocini S and Skowronek M A 1995 *J. Phys. B: At. Mol. Opt. Phys.* **28** 2021–31
[17] David N, Spence D J and Hooker S M 2004 *Phys. Rev.* E **70** 056411
[18] Semkat D, Redmer R and Bornath T 2006 *Phys. Rev.* E **73** 066406
[19] Morozov I V and Norman G E 2005 *JETP* **100** 370–84
[20] Morozov I, Reinholz H, Röpke G, Wierling A and Zwicknagel G 2005 *Phys. Rev.* E **71** 066408
[21] Weisheit J C 1988 *Adv. At. Mol. Phys.* **25** 101–31
[22] Allen P B 1987 *Phys. Rev. Lett.* **59** 1460–3
[23] Gusev V E and Wright O B 1998 *Phys. Rev.* B **57** 2878–88
[24] Volkov A E and Borodin V A 1998 *Nucl. Instrum. Methods Phys. Res.* B **146** 137–41
[25] Petrov Y V 2005 *Laser Part. Beams* **23** 283–9
[26] Lee Y T and More R M 1984 *Phys. Fluids* **27** 1273–86
[27] Kalitkin N N and Pavlov A S 2004 *Mat. Model.* **16** (12) 61–8
[28] Kalitkin N N and Pavlov A S 2005 *Mat. Model.* **17** (6) 21–32
[29] More R M, Warren K H, Young D A and Zimmerman G B 1988 *Phys. Fluids* **31** 3059–78
[30] Zel'dovich Y B and Raizer Y P 1967 *Physics of Shock Waves and High-Temperature Hydrodynamic Phenomena* (New York: Academic)
[31] Bushman A V, Fortov V E, Kanel' G I and Ni A L 1993 *Intense Dynamic Loading of Condensed Matter* (Washington, DC: Taylor & Francis)
[32] Isakov V A, Kanavin A P and Uryupin S A 2006 *Quantum Electron.* **36** 928–32
[33] Agranat M B, Andreev N E, Ashitkov S I, Veisman M E, Levashov P R, Ovchinnikov A V, Sitnikov D S, Fortov V E and Khishchenko K V 2007 *JETP Lett.* **85** 271–6
[34] Palik E D 1985 *Handbook of Optical Constants of Solids* (London: Academic)
[35] Gauthier J C, Geindre J P, Audebert P, Bastiani S, Quoix C, Grillon G, Mysyrowicz A, Antonetti A and Mancini R C 1997 *Phys. Plasmas* **4** 1811–7
[36] Grimes M K, Rundquist A R, Lee Y S and Downer M C 1999 *Phys. Rev. Lett.* **82** 4010–3
[37] Wang X Y and Downer M C 1992 *Opt. Lett.* **17** 1450–2
[38] Agranat M B, Ashitkov S I, Ivanov A A, Konyashchenko A V, Ovchinnikov A V and Fortov V E 2004 *Quantum Electron.* **34** 506–8
[39] Agranat M B, Andreev N E, Ashitkov S I, Ovchinnikov A V, Sitnikov D S, Fortov V E and Shevel'ko A P 2006 *JETP Lett.* **83** 72–4
[40] Temnov V V, Sokolowski-Tinten K, Zhou P and von der Linde D 2006 *J. Opt. Soc. Am.* B **23** 1954–64
[41] Zhang N, Zhu X, Yang J, Wang X and Wang M 2007 *Phys. Rev. Lett.* **99** 167602
[42] Takeda M, Ina H and Kobayashi S 1982 *J. Opt. Soc. Am.* **72** 156–60
[43] Sokolowski-Tinten K, Bialkowski J, Cavalleri A, von der Linde D, Oparin A, Meyer-ter-Vehn J and Anisimov S I 1998 *Phys. Rev. Lett.* **81** 224–7
[44] Andreev N E, Veysman M E, Efremov V P and Fortov V E 2003 *High Temp.* **41** 594–608
[45] Veysman M, Cros B, Andreev N E and Maynard G 2006 *Phys. Plasmas* **13** 053114
[46] Spitzer L Jr and Härm R 1953 *Phys. Rev.* **89** 977–81
[47] Andreev N E, Fortov V E, Kostin V V and Veisman M E 1996 *Proc. SPIE* **2770** 115–25
[48] Ginzburg V L 1970 *The Propagation of Electromagnetic Waves in Plasmas* (Oxford: Pergamon)
[49] Gibbon P 2005 *Short Pulse Laser Interactions with Matter* (London: Imperial College Press)
[50] Ashcroft N W and Mermin N D 1976 *Solid State Physics* vol 1 (New York: Holt, Rinehart and Winston)
[51] Thèye M L 1970 *Phys. Rev.* B **2** 3060–78
[52] Silin V P and Rukhadze A A 1961 *Electromagnetic Properties of Plasma and Plasma-like Media* (Moscow: Atomizdat)
[53] Hüttner B 1996 *J. Phys: Condens. Matter* **8** 11041–52
[54] Yakubov I T 1993 *Phys.—Usp.* **36** 365–79
[55] Abrikosov A A 1988 *Fundamentals of the Theory of Metals* (Amsterdam: North-Holland)
[56] Antia H M 1993 *Astrophys. J. Suppl. Ser.* **84** 101–8
[57] Lotz W 1968 *Z. Phys.* A **216** 241–7
[58] Fortov V E, Khishchenko K V, Levashov P R and Lomonosov I V 1998 *Nucl. Instr. Meth. Phys. Res.* A **415** 604–8
[59] Povarnitsyn M E, Itina T E, Khishchenko K V and Levashov P R 2007 *Appl. Surf. Sci.* **253** 6343–6
[60] Povarnitsyn M E, Itina T E, Sentis M, Khishchenko K V and Levashov P R 2007 *Phys. Rev.* B **75** 235414
[61] Lin Z and Zhigilei L V 2006 *Proc. SPIE* **6261** 62610U
[62] Lin Z and Zhigilei L V 2007 *Appl. Surf. Sci.* **253** 6295–300
[63] Guo C, Rodriguez G, Lobad A and Taylor A J 2000 *Phys. Rev. Lett.* **84** 4493–6